FCAL d+Au Centrality Analysis

Jason Newby, Akitomo Enokizono, Mike Heffner, Stephen Johnson, Jennifer Klay, and Ron Soltz

March 22, 2005

1 Introduction

In Au+Au collisions in PHENIX, the charged particle multiplicity in the beam-beam counters is used to extract centrality. This method has also been applied in d+Au (d+Au) collisions for high-p_T analyses. These are biased by the correlation of hadron multiplicity in the south BBC and a hard scattering that produces a high-p_T particle[1]. The centrality of a d+Au collision might be characterized in many ways, but must ultimately be correlated with an experimental observable. The BBC centrality analysis assumes BBC multiplicity scales linearly with the number of Au participants. Another common method to extract N_{part}, N_{coll} in p-A reactions is to parameterize the dependence of the mean number of recoil protons (N_{grey}) with the number of target participants [2]. The Forward Hadron Calorimeter (FCAL) was installed prior to the RHIC d+Au run to measure the energy of these free protons swept out of the beam line by the RHIC DX magnet. We present here a method of centrality determination using the energy spectrum of the Forward Hadron Calorimeter for d+Au collisions recorded in RHIC year 3.

2 The FCAL Detector and Energy distribution

The concept to operation time of the FCAL was only 6 months, just in time for the first d+Au collisions. The commissioning run for the new detector was also the physics run for our analysis. While the FCAL team quickly addressed detector problems during the changing run conditions, some peculiarities of the detector hardware and backgrounds have only been uncovered in the offline analysis.

- A reset operation in the readout electronics resulted in the corruption of approximately one-tenth of the physics data. No meaningful information can be recovered from these recorded events. The observable symptom identifying this operation is the anomalous behavior in the ZDC-FCAL correlation compared to the typical situation demonstrated in Figure 1. Fortunately, these events are not correlated with any physics trigger and disregarding these events does not bias analyses in any way. There are 120 buckets in the RHIC machine which can be filled with ions. Approximately ten consecutive buckets called the "abort gap" are left

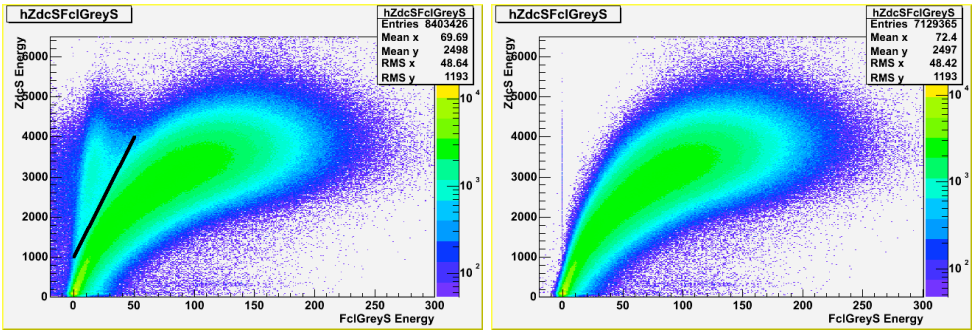

Figure 1: The analog reset operation results in a disagreement of the FCAL with the typical ZDC correlation. The left panel includes all minimum-bias events including those above the sketched line where the analog reset was executed. The right panel excludes beam crossings [11, 35].

empty to facilitate the beam dump. The reset operation was issued just before the abort gap at bucket 11. All events recorded in buckets 11 through 35 are excluded from the FCAL analysis.

- For each 100GeV neutron shower in the Zero-Degree Calorimeter, approximately 1.5 GeV of energy is absorbed by the FCAL. The FCAL and ZDC are both located just beyond the diverging beams separated only by the material of one beam pipe. Of the nine columns of modules in the FCAL, the modules closest to the beam pipe are the most susceptible to this cross-talk. The break-up of the Au nucleus even in peripheral collisions produces a large neutron multiplicity. This ZDC cross-talk shifts the FCAL energy distribution in each module proportional to the ZDC energy. The correlation is determined on a module-by-module basis and subtracted event-by-event as documented in TN413[3].

- As the luminosity of the collider improved during the beginning of the run, the increased rate of collision related signal in the FCAL detector became comparable to the relaxation time of the charge integrator of the readout electronics. The shift of the baseline reduced the dynamic range and pushed the signal into a region of non-linearity. The solution devised for this problem was to reset the baseline every beam cycle, 120 RHIC clocks tics or 13μs. In reality this only masked a saturation caused by coupling of charge buildup on an intervening high-pass filter capacitor and a voltage clamp with a lower limit of -4V and upper limit of 0V. The level of saturation is determined by the signal rate for each module. This is determined by both the collision rate, which varied dramatically over the run and within a each RHIC fill, and the distance of the module from the beam-pipe. This effect is demonstrated for two FCAL modules in Figure 2. We have quantified this effect for each channel and removed channels with more than a 5% dependence shown in Figure 3.

After correcting for these effects, the total energy distribution for the subset of useful modules is shown for a minimum bias (BBCLL1) distribution in Figure 2.

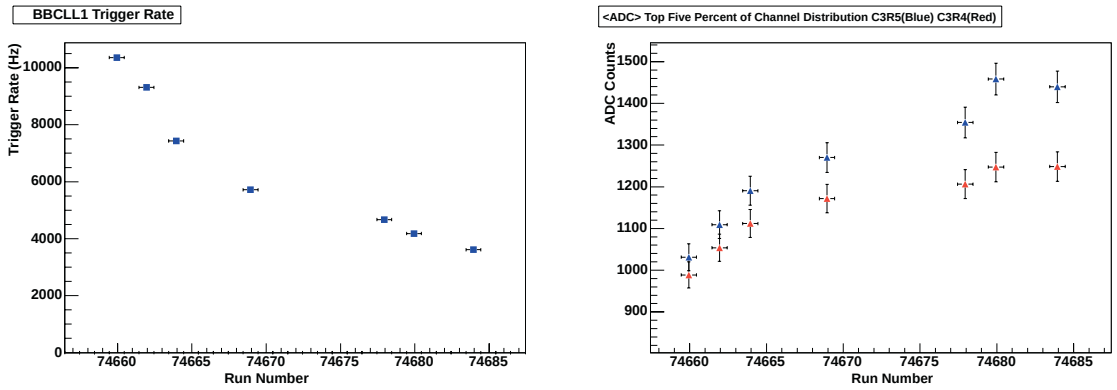

Figure 2: The rate dependence of saturation in two FCAL modules is demonstrated in the trends shown. In the left panel, the BBC rate averaged over a run is shown over the course of a RHIC d+Au fill. In the right panel, the average un-calibrated gains (ADC counts) for the top 10% of the distributions are shown for the two center modules in the third column of the FCAL. Ideally, the $\langle ADC_{Top10\%} \rangle$ would be independent of rate; however, we see a dependence of as much as 40% over the course of the RHIC fill.

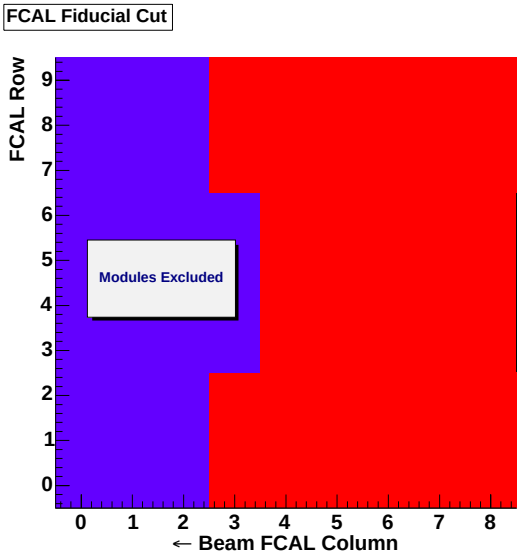

Figure 3: Modules excluded from south FCAL centrality analysis.

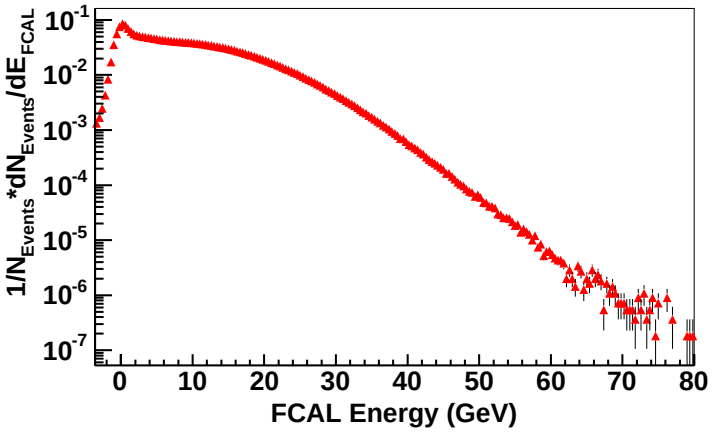

Figure 4: FCAL energy sum excluding columns[0-2] + column3 rows[3-6].

3 Run 3 Centrality Reconstruction

The FCAL sums calculated in the original data production are not sufficient to reconstruct the Run3 centrality for three reasons.

- Due to a bug in the original production calibration code, the first two rows of both FCAL detectors were not corrected for channel-by-channel gain differences.
- The original sums, FclETotl and FclEGrey, included channels that were demonstrated to be strongly saturated.
- The ZDC-XTalk correction should be applied on a channel-by-channel basis to evaluate run-by-run variations.

This channel-by-channel information was not stored in any of the nanoDST's in the PHENIX run3 production. We had to return to the DST's archived in HPSS requiring a lengthy production project. We staged 229 runs of the total 510 in the good run list from PHENIX run3dAu_v03_pro45 and run3dAu_v03_pro47 productions. The FCAL production gave priority to the larger runs and to those used in the PPG036 analysis. Each DST was staged and processed with the macro offline/packages/fcl/macros/runRecal.C. The resulting nanoDST included the following objects: Sync, TrigLvl1, PHGlobal, fclRawNorth, fclRawSouth. These tables are chosen to provide the following features: The TrigLvl1 object provides information necessary for selecting minimum-bias events to produce a minimum-bias FCAL energy spectrum. The PHGlobal object includes vertex information and BBC centrality for comparison. The Sync object facilitates the matching of every event to the corresponding event in another PHENIX analysis nanoDST such as CNT and MWG such that the latter can be dynamically merged with the FCAL nanoDST in the Fun4All framework to provide FCAL centrality to these analyses. The raw FCAL data is recorded so that all corrections

may be later applied in a recalibrator module. The calibrations and correction enumerated above are calculated by the module, offline/packages/fcl/FclRecal.

4 Binary Collision Extraction

The interest in the centrality dependence of most physics observables is based on an expected scaling with either the number of participating nucleons (N_{part}) or the number of binary nucleon-nucleon collisions (N_{coll}). For d+Au reactions this has been done using the Au-side (south) BBC multiplicity distribution and documented in analysis note 210 [4]. The approach taken in that analysis is to divide the BBC multiplicity distribution into four bins: 23% for the most central bins and 32% for the most peripheral bin. For each centrality class the quantities $\langle N_{part} \rangle$, $\langle N_{coll} \rangle$ are determined. The procedure is summarized below.

1. A glauber model is used to generate an unbiased N_{coll} and N_{part} distribution for the d+Au nuclear geometry.
2. The glauber distributions are modified to include the trigger bias of the BBCLL1.
3. The $P(N_{Hits,BBC}|N_{part,Au})$ distribution is assumed to be a Negative-Binomial distribution.
4. The $P(N_{Hits,BBC}|N_{part,Au})$ is weighted with the trigger-biased glauber distribution to fit the measured $N_{Hits,BBC}$ distribution.
5. The conditional distribution $P(N_{Hits,BBC}|N_{part,Au})$ is inverted to obtain the $P(N_{part,Au}|N_{Hits,BBC})$ distribution.
6. The $P(N_{part,Au}|N_{Hits,BBC})$ is weighted with the measured $N_{Hits,BBC}$ distribution and integrated separately over each centrality class.

The binary collision extraction from the FCAL was guided both by observations of previous experiments and calculations with a full PISA simulation. The Statistical Multi-fragmentation Model (SMM) [5, 6] was used to calculate realistic proton and neutron kinematic distributions. To fit the FCAL energy distribution a procedure similar to the BBC analysis is used except that item 3 is substituted with the Gamma distribution described in equation 1. The significance of parameters k and λ are described later.

$$f(E_{FCAL}|\lambda, k) = \frac{E_{FCAL}^{k-1} \lambda^k e^{-\lambda E_{FCAL}}}{\Gamma(k)} \tag{1}$$

The simulated FCAL response is well described by the Gamma distribution. The FCAL response for fixed values of grey proton multiplicity, N_{grey}, is shown Figure 5 with the independently fitted Gamma distributions. An important property of the Gamma distribution is that the convoluted sum of N Gamma distributions is itself a Gamma distribution with $k \rightarrow N \times k$ [7]. The fit parameters for a range of N_{grey} are shown in Figure 6. As expected, the Gamma k parameter rises linearly while the $1/\lambda$ parameter remains constant. This demonstrates in principle that the energy

Table 1: Centrality Analysis Comparison

BBC	FCAL
Glauber	Glauber
BBCLL1 Bias	BBCLL1 Bias
NBinomial	Gamma
high p_T Bias Correction	no Bias correction

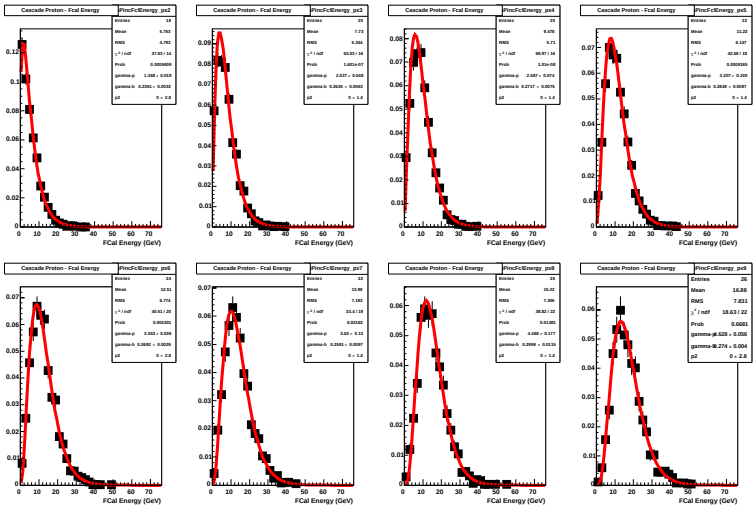

Figure 5: Energy Distributions for events with fixed N_{grey} ranging from 2-9 and corresponding fits with a Gamma distribution.

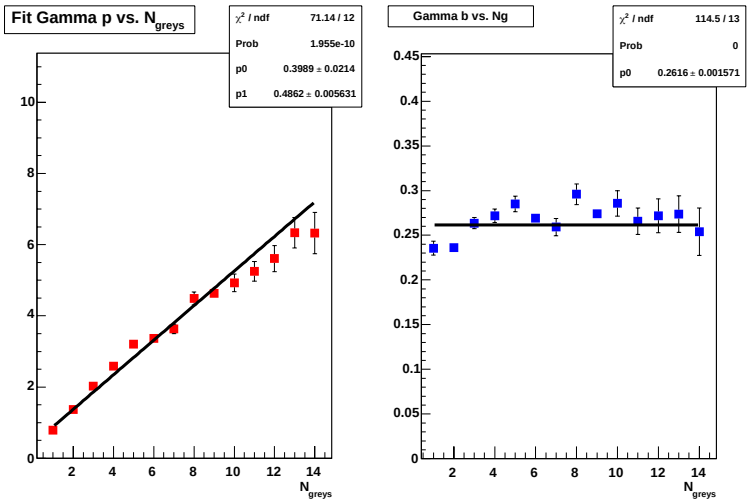

Figure 6: For each value of N_{grey} the parameters ($p \rightarrow k$,$b \rightarrow 1/\lambda$) of the Gamma distribution fits to the simulated response are shown.

distribution is enough to determine the conditional probability distribution $P(N_{grey}|E_{FCAL})$ if we know, $P(N_{grey})$.

In reality, we do not know $P(N_{grey})$ for the 200 GeV/c d+Au system. However, experiments for p+Au collisions at lower energies give some insight. We must make one assumption: the number of participating target nucleons may be determined from a nuclear geometry model. For the d+Au system we use the standard PHENIX offline/analysis/glauber_mc code with default Au parameters. The systematic uncertainties associated with variation of the model parameters are considered in Table 3. Previous experiments have explored the correlation between the number of participants and the number of grey protons, $\langle N_{grey}\rangle(N_{part})$ [2]. In the E910 analysis, a second order polynomial was used to fit the $\langle N_{grey}\rangle(N_{part})$ dependence. This was motivated by two phenomenological approaches: one predicted a linear dependence [8] and another a quadratic dependence [9]. An important result of the E910 measurement is that not only did the linear dependence dominate, but the extracted coefficient of the quadratic term was negative. One explanation is a saturation in the participant scaling of the cascade proton multiplicity.

The natural convolution of the energy response $P(E_{FCAL}|N_{grey})$, the proton multiplicity $P(N_{grey}|N_{part})$, and the underlying Glauber participant distribution, $\pi(N_{part})$ follows:

$$P(E_{FCAL}) = \sum_{N_{part}=1}^{\infty} \pi(N_{part}) \times \sum_{N_{grey}=0}^{\infty} P(N_{grey}|N_{part}) \times P(E_{FCAL}|N_{grey}) \qquad (2)$$

If the parameters for $P(N_{grey}|N_{part})$ and $P(E_{FCAL}|N_{grey})$ are extracted from separate fits to the corresponding simulated distributions, the subsequent convolution of the form of Equation 2 well describes the total simulated energy distribution of the FCAL. However, there are 3 or more param-

eters for $P(E_{FCAL}|N_{grey})$, and the $P(N_{grey}|N_{part})$ has a fixed total population parameter, Z_{Au} and a parameter, $\langle N_{grey}\rangle$, with a parameterized dependence on N_{part} requiring typically 3 parameters. In this form, there are 6 fit parameters, which are not entirely independent, such that χ^2 minimization does not reliably converge. We reduce the number of parameters by folding the narrower Binomial multiplicity distribution of $P(N_{grey}|N_{part})$ into the Gamma distribution and reducing $P(N_{grey}|N_{part})$ to $\langle N_{grey}\rangle(N_{part})$. The effect of this simplification is illustrated in Figure 7 and the simplified probability distribution is

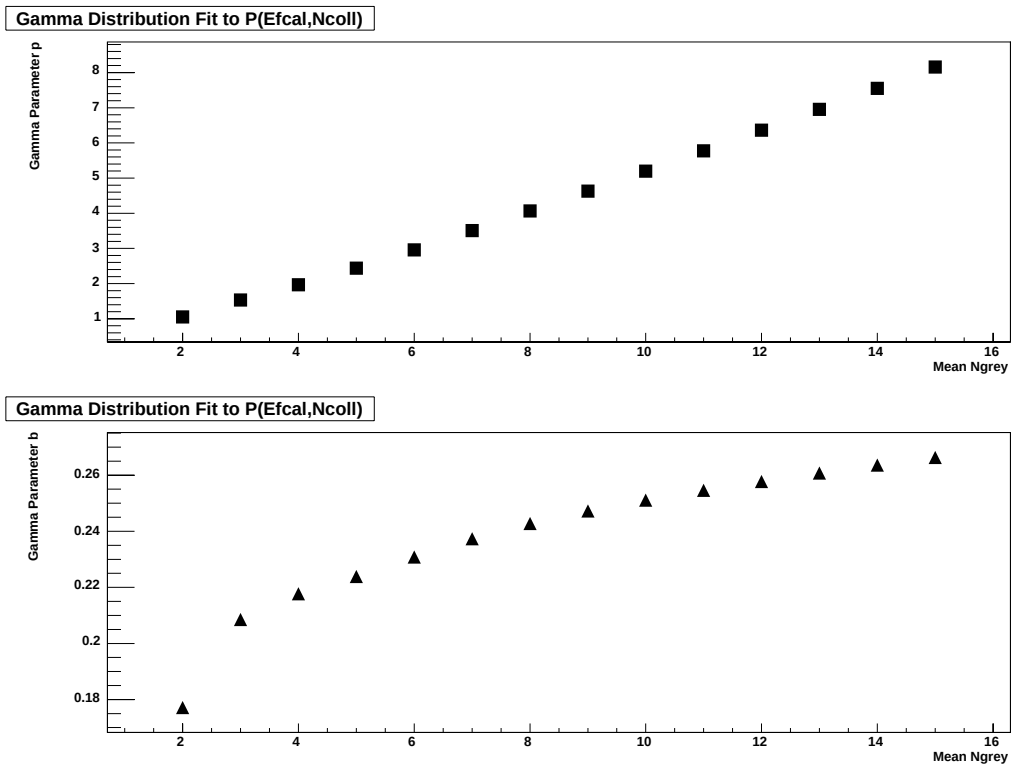

Figure 7: The Gamma distribution when convoluted with a binomial distribution does not result in a Gamma distribution, but may be fit with a Gamma distribution for large Gamma parameter p. Shown are the Gamma fit parameters p and b to such a convolution where the input Gamma distribution parameter b is 0.5 and the input parameter p corresponds to Mean Ngrey.

$$P(E_{FCAL}) = \sum_{N_{part}=1}^{\infty} P_{Glauber}(N_{part}) \times P(E_{FCAL}|N_{part}) \tag{3}$$

where $P(E_{FCAL}|N_{part})$ is the gamma distribution of Equation 1 with parameters $\lambda \sim \langle E_{FCAL,N_{grey}=1}\rangle$ and $k(N_{part}) = \langle N_{grey}\rangle(N_{part})$. Instead of the strictly linear relationship demonstrated in Figure 6, we accommodate the quadratic term of $\langle N_{grey}\rangle(N_{part})$ into a quadratic term for $k(N_{part})$.

5 Centrality Results

The probability distribution described in Equation 3 is fit to the FCAL energy distribution of the run3 d+Au minimum-bias data set. We have tried a variety of parameterizations for $\langle N_{grey}\rangle(N_{part})$. In all cases, the freedom to saturate at large N_{part} was favored. We consider two functional forms

$$\langle N_{grey}\rangle(N_{part}) = \quad a_0 + a_1 \times N_{part} + a_2 \times N_{part}^2 \quad (poly2) \tag{4}$$

$$\langle N_{grey}\rangle(N_{part}) = \quad a_0 \times [1 - \exp(-(N_{part}/a_1)^{a_2})] \quad (SS2) \tag{5}$$

A strong saturation component was essential for describing the data before excluding saturating FCAL channels motivating the SS2. With the energy response of the FCAL now better understood, the polynomial remains the simplest and most effective in fitting the corrected FCAL energy spectrum. By varying the functional forms we estimate the systematic error from assuming a parameterized $\langle N_{grey}\rangle(N_{part})$ shown in Table 2. We have yet another handle on the systematic error of our model. While the product of this work is an centrality determination for the minimum bias data set, the neutron-tagged sample provides a very different collision geometry on which to test the assumptions of our model[4]. These are d+Au collisions in which only the projectile proton interacts with the Au nucleus. The projectile spectator neutron is then detected in the North ZDC. By requiring at least 40 GeV in the North ZDC, this class of events are isolated. The fits to the minimum bias sample and the neutron-tagged sample are shown in Figure 8. We use one alternate functional form (SS2) to estimate the systematic errors associated with the choice of functional form for the $N_{part,Au}$ dependence of the mean FCAL energy.

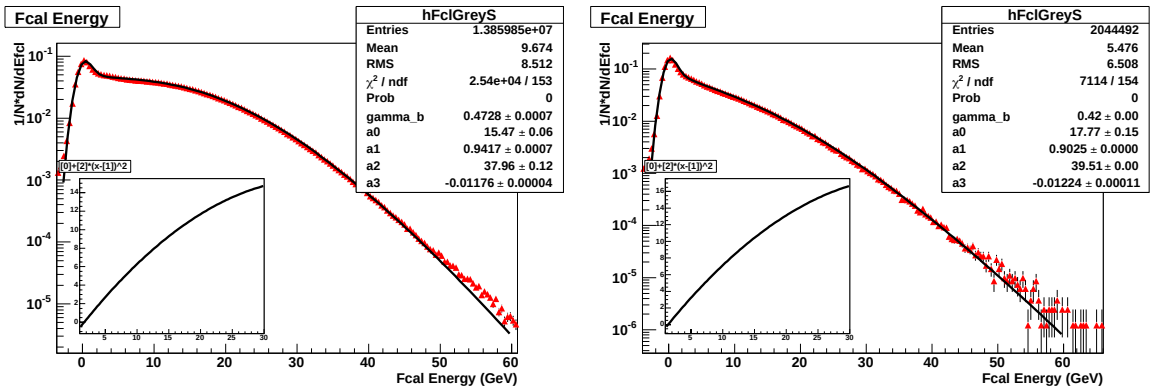

Figure 8: The FCAL energy distributions and fits are shown for the minimum-bias sample(left) and the neutron-tagged sample(right). Inset in each panel is the extracted relation,$\langle N_{p,cascade}\rangle(N_{part})$.

The fit parameters to the total FCAL energy distribution are then used in the utiCentralityFcal class to calculate the $N_{part,Au}$ probability distribution on an event-by-event basis. These distributions are summed within the four centrality classes defined by the FCAL energy. The $N_{part,Au}$ distribution is then converted to the N_{coll} distribution using the Glauber $N_{coll} - N_{part,Au}$ correlation, $G_{N_{coll}N_{part,Au}}$ and the N_{coll} BBC efficiency[4].

Table 2: Systematic Error Estimate

Ncol	SS2	SS2 N_{tag}	Poly2	Poly2 N_{tag}	%Diff Max-Min
0-20	13.93	13.1	15.21	13.54	15%
20-40	11.63	11.26	11.19	9.5	20%
40-60	8.11	7.72	7.55	6.26	25%
60-88	3.35	2.88	3.22	2.74	20%
Ncol Ratio					
0-20	4.16	4.55	4.72	4.94	17%
20-40	3.47	3.91	3.48	3.47	12%
40-60	2.42	2.68	2.34	2.28	16%
NpartAu					
0-20	12.66	11.81	13.95	12.26	17%
20-40	10.45	10.11	9.96	8.38	21%
40-60	7.19	6.87	6.63	5.49	26%
60-88	2.95	2.53	2.83	2.41	20%

$$P_{N_{coll}} = \epsilon_{N_{coll}} G_{N_{coll} N_{part,Au}} P_{N_{part,Au}} \tag{6}$$

Systematic errors associated with our model are estimated in part by comparing the parameters fit to the minimum bias FCAL distribution and the parameters fit to the neutron-tagged sample. The parameter sets for both trigger samples and both functional forms were used to extract the $\langle N_{part} \rangle$, $\langle N_{coll} \rangle$ for four centrality classes binned in FCAL energy. These are tabulated in Table 2 along with the variations in the ratios of the three more central classes to the most peripheral class. The largest systematic uncertainty is for the 0-20:60-88 ratio of 17%. For the minimum-bias neutron-tagged comparison, one parameter for both functional forms was fixed to the value of the minbias fit. In both cases, this is related to the $\langle N_{grey} \rangle$ saturation value for large values of N_{part}. It is unphysical to force the saturation value derived from the fit to the neutron-tagged distribution upon the minimum bias distribution.

The FCAL energy distribution includes some contribution from black protons from fragmentation/evaporation that are correlated to the number of participants very differently from the cascade protons. In fact the evaporation protons have a relatively fast rise similar to the evaporative neutrons and quickly saturate in peripheral collisions as shown in Figure 9. We estimate the systematic uncertainty from this contribution using the Statistical Multifragmentation Model (SMM) to generate d+Au collisions with a full PISA simulation of both the protons and neutrons. From the model, we can explicitly identify the energy contribution to the FCAL from the cascade protons and the evaporative protons. The effect is to shift the energy distribution to higher energy. Since the evaporative protons saturate very quickly, most of the effect is in the peripheral collisions. For this simulated data, we extract the $\langle N_{part} \rangle$ for the four centrality bins for two cases. In the first case, we include only the contribution of the protons from the binary cascade stage of the model to the FCAL energy distribution. In the second case, we include both the previous component and the contribution from the later fragmentation/evaporation stage. The contribution of the fragmentation/evaporation proton energy results in an overestimate of the ratio $N_{part,cent}/N_{part,periph}$ by 7

Table 3: $\langle N_{coll} \rangle$ Glauber d+Au

	0-20%		20-40%		40-60%		60-88%	
Runtype	$\langle N_{coll} \rangle$	RMS	$\langle N_{coll} \rangle$	RMS	$\langle N_{coll} \rangle$	RMS	$\langle N_{coll} \rangle$	RMS
default	15.5	4.3	10.5	3.8	6.7	3.3	3.1	2.2
σ_{tot}*1.05	15.5	4.3	10.5	3.8	6.7	3.3	3.2	2.2
σ_{tot}*0.95	15.5	4.3	10.5	3.8	6.7	3.3	3.0	2.2
Gaussian	15.7	4.4	10.3	3.7	6.3	3.0	2.8	2.0
Gray	15.5	4.3	10.4	3.7	6.5	3.2	3.0	2.1
Hulthen*1.1	15.8	4.4	10.8	3.9	6.8	3.4	3.1	2.2
Hulthen*0.9	15.4	4.3	10.3	3.7	6.4	3.2	3.0	2.1
σ_{NN} - 3mb	14.6	4.1	9.8	3.6	6.2	3.1	3.0	2.1
σ_{NN} + 3mb	16.5	4.5	11.2	4.1	6.9	3.4	3.1	2.3
Woods-Saxon Larger	15.4	4.3	10.5	3.8	6.6	3.3	3.1	2.2
Woods-Saxon Smaller	15.7	4.4	10.5	3.9	6.6	3.3	3.0	2.2

% for all three ratios of central to the most peripheral centrality classes.

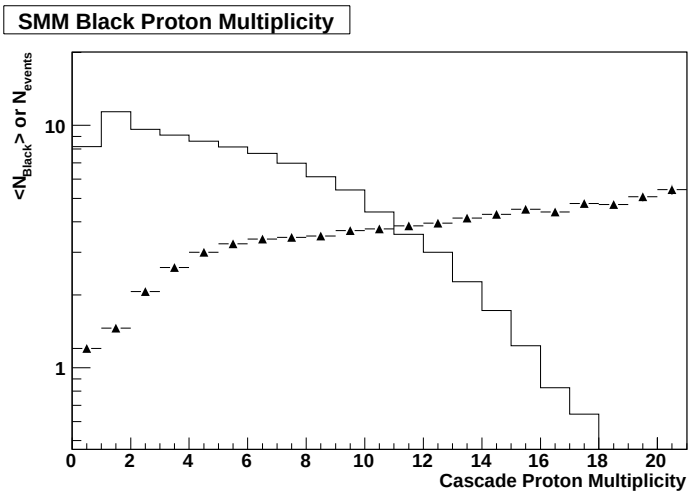

Figure 9: The SMM calculation of the mean black proton multiplicity $\langle N_{black} \rangle$ (triangles) and the cascade multiplicity distribution (solid line) for d+Au collisions.

The assumption of the Glauber nuclear geometry model described in [10] introduces an additional systematic error. The variation in the participant and binary collision distributions with geometry parameters has been studied and is tabulated in Tables 3and 4. As in previous d+Au analyses [4], the uncertainty in the nucleon-nucleon cross section yields the greatest variations in the number of participants, binary collisions, and the corresponding ratios of centrality event classes. This also dominates the Glauber model contribution to the overall systematic uncertainty. We include any correlated systematic uncertainty in the binary collision ratios ratios by explicitly calculating the ratios and then adding the maximum variation about the mean in quadrature shown in Table 7.

Table 4: $\langle N_{part}^{Au} \rangle$ Glauber d+Au

Runtype	0-20% $\langle N_{part}^{Au} \rangle$	RMS	20-40% $\langle N_{part}^{Au} \rangle$	RMS	40-60% $\langle N_{part}^{Au} \rangle$	RMS	60-88% $\langle N_{part}^{Au} \rangle$	RMS
default	14.2	3.8	9.3	3.0	5.8	2.7	2.7	1.8
σ_{tot}*1.05	14.2	3.8	9.3	3.0	5.8	2.7	2.8	1.9
σ_{tot}*0.95	14.2	3.8	9.3	3.0	5.8	2.7	2.6	1.8
Gaussian	14.4	3.8	9.4	3.1	5.7	2.6	2.6	1.8
Gray	14.2	3.8	9.3	3.1	5.8	2.6	2.7	1.8
Hulthen*1.1	14.3	3.9	9.3	3.1	5.8	2.6	2.7	1.8
Hulthen*0.9	14.2	3.9	9.2	3.0	5.7	2.6	2.7	1.8
σ_{NN} - 3mb	13.4	3.7	8.7	2.9	5.5	2.5	2.7	1.8
σ_{NN} + 3mb	15.1	4.0	9.8	3.2	6.1	2.7	2.8	1.9
Woods-Saxon Larger	14.1	3.8	9.2	3.0	5.8	2.6	2.7	1.8
Woods-Saxon Smaller	14.4	3.9	9.3	3.1	5.8	2.6	2.7	1.8

Table 5: $\langle N_{coll} \rangle$, $\langle N_{part}^{Au} \rangle$ Glauber d+Au Systematics

Centrality	$\langle N_{coll} \rangle$	RMS	Systematic Variation	$\langle N_{part}^{Au} \rangle$	RMS	Systematic Variation
0-20%	15.5	4.3	1.1 (7.0%)	14.2	3.8	0.9 (6.7%)
20-40%	10.5	3.8	0.8 (7.6%)	9.3	3.0	0.6 (6.7%)
40-60%	6.7	3.3	0.7 (11.1%)	5.8	2.7	0.3 (5.7%)
60-88%	3.1	2.2	0.4 (12.1%)	2.7	1.8	0.2 (6.4%)

Table 6: R_{CP} Glauber d+Au Systematics

R_{CP}	$\langle N_{coll} \rangle$	$\langle N_{part}^{Au} \rangle$
(0-20%)/(60-88%)	5.00 ± 0.77 (15.5%)	5.3 ± 0.5 (8.8%)
(20-40%)/(60-88%)	3.39 ± 0.42 (12.4%)	3.4 ± 0.3 (9.1%)
(40-60%)/(60-88%)	2.16 ± 0.16 (7.3%)	2.1 ± 0.1 (7.0%)

Table 7: Centrality R_{CP} Systematic Uncertainties

Source	0-20%	20-40%	40-60%
Cascade Proton Model	17%	12%	16%
Black Protons	7%	7%	7%
Glauber	16%	12%	7%
Quadratic Sum	24%	18%	19%

6 Nuclear Modification Factors using the FCAL Centrality

6.1 Introduction

The nuclear modification factors in d+Au collisions have been measured by PHENIX in PPG036 using the forward muon spectrometers. At the time of its publication, centrality determination with the FCAL was not yet available and the analysis proceeded utilizing the multiplicity in the Au-side beam-beam counter. The PPG036 analysis measured hadron production at forward and backward rapidity using two very different methods, statistical isolation and explicit identification. Many hadrons produced in the collision decay to muons in flight before reaching the 4.9 interaction-length absorber. Since the mean path before decay is much larger than the distance to the absorber, the probability of decaying before the absorber is linearly dependent on the distance of the collision vertex from the absorber. By comparing the muon production at vertices near the absorber to those far from the absorber, the decay muon component is statistically isolated and detailed in AN345 [11]. These spectrometers were designed to be inefficient for hadrons to enhance the purity of the muon sample. Nevertheless, some high momentum pions "punch through" the absorber and are tracked through the spectrometer as pions. Since muons interact only electromagnetically, the strong interactions of pions with the absorber cause them to range out much earlier than a muon of the same momentum. By considering a sample of muons and pions that range out at the same depth in the MuID, they may be separated by their momentum as detailed in AN343 [12]. The sensitivity of this analysis to BBC centrality correlations described in AN342 makes a comparison with an FCAL centrality analysis particularly attractive.

6.2 Centrality Dependence with the FCAL

In the present analysis, we are guided by AN343 and repeat the R_{CP} measurement for only the "punch through" hadron 1D triggered sample, substituting the FCAL centrality classes for those of the BBC and the corresponding $\langle N_{coll} \rangle$ values from section 5. This final analysis of the original analysis was carried out on a set of Ntuples produced by the analysis module MuonNdstAna in offline/packages/mutoo_subsysreco. The data sets considered for this analysis are a subset of those in AN343 and are listed in Appendix A. To incorporate the FCAL centrality information, we added the variable T_centfcl to the Ntuple calculated using the getdAuCentralityPercentile method of the FCAL centrality class utiCentralityFcal in offline/packages/uti. The centrality calculation uses the calibrated and ZDC-Xtalk subtracted FCAL South energy sum computed by the FclRecal recalibration module in offline/packages/fcl.

The event selection and single track cuts from AN343 Table 6 are summarized in Table 8. One single track cut of AN343 that was not exactly duplicated is the matching of MuID roads to tracks at gap 0 of the MuID, $R_{proximity}$. The cut on this track quality parameter was added after the Quark Matter 2004 analysis. The code utilized in the original analysis to calculate the Track-Road matching at MuID Gap 0 has been integrated into a utility library in method Tools::DG0. The $R_{proximity}$ track parameter is the distance in the plane of MuID Gap 0 between the projection of the MuTr Track and the MuID road at Gap 0. In Figure 10, the $R_{proximity}$ distributions are shown for both North and South muon arms when all other track quality cuts have been applied.

Table 8: Event and Track Cuts

Cut	Value
z_vtx	[-28,+28]
χ^2	< 20
p_{tot}^{st1}	>1.8
p_T	[1.5, 4.0]
θ_{xp}	< 0.03
$DG0$	< 30 cm

For consistency with previous analyses, we require $R_{proximity} < 30$cm and that the hadron be in coincidence with a level 1 trigger for the corresponding muon arm.

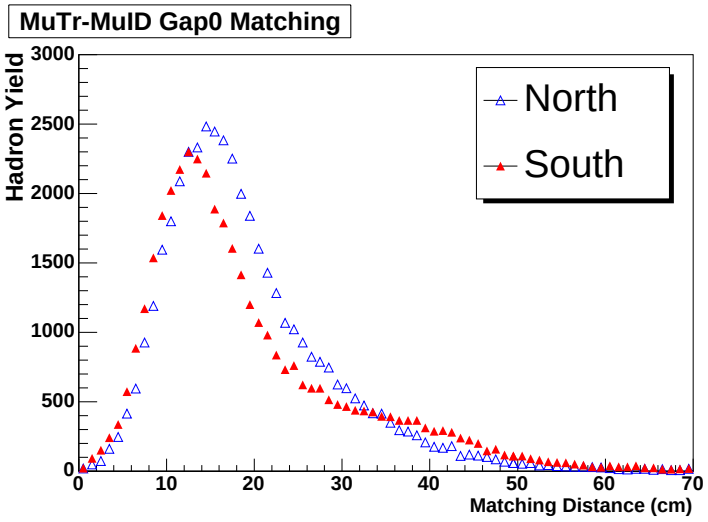

Figure 10: The $R_{proximity}$ parameter for MuTr-MuID matching at gap 0 of MuID.

The systematic uncertainties for the included cuts for each centrality class may be found in Table 5.4 of AN343. Most of the corrections and systematic uncertainties determined in AN343 are applicable to the FCAL centrality analysis, but there are some important differences. In the BBC centrality analysis there are two separate corrections that must be made for the BBC bias. The first is the trigger bias introduced by the BBCLL1 trigger. This effect is greatest in the most peripheral event where the efficiency of triggering on low multiplicity reactions is smallest. The second effect is the correlation with centrality binning of the BBC multiplicity with a high-p_T pion. The events on the the high multiplicity edge of a peripheral BBC centrality bin is more likely to be shifted to the more central bin if a high-p_T pion is present. Since the FCAL analysis is using the same BBCLL1 triggered sample as the BBC centrality analysis, the first correction is still applicable to the FCAL centrality analysis and is included in the FCAL results. The FCAL does not measure produced particles but instead a combination of spectators and participants. The FCAL response is correlated to the number of participants independent from the particle production. The latter BBC bin-shifting correction is therefore not applied to the FCAL centrality analysis. The corrections applied in the FCAL analysis and the BBC comparison are taken from Table 2 of AN342 and

Table 9: Bias Corrections C_i

Analysis	0 - 20%	20 - 40%	40 - 60%	60-88%
BBC North	0.96	0.99	1.03	1.02
BBC South	0.95	0.99	1.04	1.05
FCAL	1.00	0.99	0.97	0.94

summarized here in Table 9.

6.3 Results

In this analysis we consider the pseudorapidity dependence of pion production within the acceptance of the PHENIX muon spectrometers. The same p_T range and pseudorapidity binning of AN343 is used. The raw hadron spectrum, N_i, from each of the four FCAL centrality classes is shown in Figure 11. The Nuclear Modification Factor is determined by the following equation:

$$R_{CP} = \frac{C_{cent} \times N_{cent}/N_{coll,cent}}{C_{periph} \times N_{periph}/N_{coll,periph}} \tag{7}$$

The R_{CP} values are shown for both the BBC and FCAL centrality analysis in Figure 12. Note the smaller N_{coll} ratios than that of the BBC analysis are indicative of the FCAL may having somewhat less centrality resolution than the BBC. The effect of this would be to reduce any centrality dependent effect. This is consistent with the fact that the backward enhancement for the FCAL centrality is consistently less than the BBC values and the forward suppression is consistently less dramatic. The FCAL centrality bins are determined independent of any model used to assign the $\langle N_{coll} \rangle$. The event class determination would not change, therefore a change in the $\langle N_{coll} \rangle$ ratio would move both the forward and backward R_{CP}'s collectively upward or downward. Nevertheless, the FCAL result is consistent with the BBC analysis within statistical and systematic errors.

7 Conclusions

The first d+Au centrality analysis at RHIC utilizing forward calorimetry is presented. The PHENIX FCAL measured protons in the fragmentation region. We have used the recorded energy to define four event classes and extract the mean number of binary nucleon-nucleon collisions for each centrality class. We have examined the differences of high transverse-momentum pion production at forward and backward rapidity for these centrality classes and observed deviation from binary scaling. The observation of enhancement at backward rapidity and suppression at forward rapidity with increasing centrality is consistent with the observation in the BBC centrality analysis. The energy resolution of the calorimeter in the run 3 configuration results in broader centrality bins compared to the BBC centrality class determination which appears to reduce the magnitude of the observed deviation from binary scaling. Nevertheless, we have demonstrated an alternative centrality reconstruction that is immune to many of the biases of the BBC method. With our current optimization of operational parameters, the improved FCAL resolution should provide a viable alternative to centrality determination in future p(d)+Au runs.

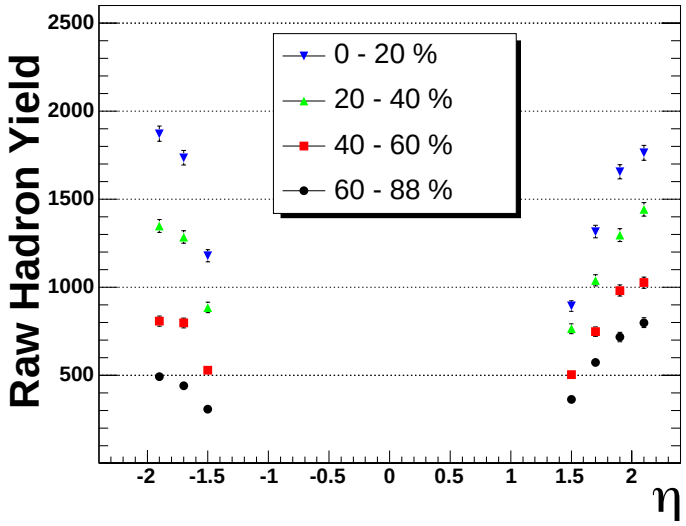

Figure 11: The pseudo-rapidity distributions of the raw number of hadron counts is plotted for each of the four centrality class determined by the FCAL for the MuID 1D trigger sample.

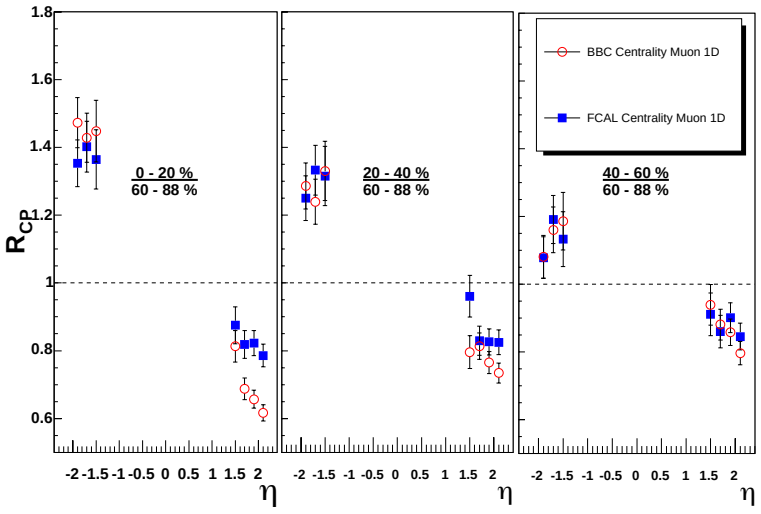

Figure 12: The nuclear modification factor, R_{CP}, for pion production is measured at forward and backward rapidity. The BBC Mulitiplicity and FCAL Energy centrality determination techniques are compared.

References

[1] C. Zhang and J. L. Nagle. Centrality determination in deuteron-gold reactions using the beam-beam counter. Analysis Note 342, PHENIX, December 2005.

[2] I. Chemakin et al. Measuring centrality with slow protons in proton nucleus collisions at 18-gev/c. *Phys. Rev.*, C60:024902, 1999.

[3] J. Newby, A. Enokizono, M. Heffner, J. Klay, and R. Soltz. Fcal calibration procedure. Technical Note 413, PHENIX, 2005.

[4] Axel Drees, Tom Hemmick, Barbara Jacak, Jiangyong Jia, Sean Leckey, Sasha Milov, Mike Reuter, Anne Sickles, and Ron Soltz. Phenix an210: Centrality determination and p_t centrality dependence in d-au collisions. Analysis Note 210, PHENIX, June 2003.

[5] J. P. Bondorf, A. S. Botvina, A. S. Ilinov, I. N. Mishustin, and K. Sneppen. Statistical multifragmentation of nuclei. *Phys. Rept.*, 257:133–221, 1995.

[6] A. S. Botvina. Private communication smm source code, 2004.

[7] M. J. Tannenbaum. The distribution function of the event-by-event average p(t) for statistically independent emission. *Phys. Lett.*, B498:29–34, 2001.

[8] Bo Andersson, Ingvar Otterlund, and Evert Stenlund. On the correlation between fast target protons and the number of hadron - nucleon collisions in high-energy hadron - nucleus reactions. *Phys. Lett.*, B73:343, 1978.

[9] M. K. Hegab and J. Hufner. How often does a high-energy hadron collide inside a nucleus? *Phys. Lett.*, B105:103–106, 1981.

[10] M. Chiu, J. Nagle, D. Morrison, S. Mioduszewski, and K. Reygers. Determining the number of participants using a hybrid glauber model approach. Analysis Note 18, PHENIX.

[11] M.L. Brooks, D. Brown, V. Cianciolo, V. Dzordzhadze, S. Gadrat, A. Glenn, Y. Kwon J.H. Kang, D.M. Lee, M.K. Lee, M.X. Liu, B. Norman, W.J. Park, K.F. Read, G. Roche, H.D. Sato, A. Taketani, T.L. Thomas, and X.R. Wang. Rcp measurement with muons from light meson decays in dau collisions at $\sqrt{S_N N} = 200\text{gev}/c^2$ at rhic. Analysis Note 345, PHENIX, December 2004.

[12] Thomas K Hemmick, Hugo Pereira, Sean Kelly, James Nagle, Anuj Purwar, and Chun Zhang. Charged hadron r_{CP} measurement in the phenix muon arm. Analysis Note 343, PHENIX, July 2004.

A Centrality Run List

77530, 77678, 77687, 77688, 78035, 78181, 78182, 78207, 78208, 78210, 78269, 78306, 78402, 78508, 78509, 78510, 78511, 78512, 78532, 78549, 78553, 78578, 78632, 78633, 78817, 78838, 78839, 79047, 79050, 79066, 79067, 79340, 79560, 79615, 79626, 79629, 79630, 79632, 79641, 79642, 79740, 79762, 79872, 79875, 79885, 79888, 79960, 79961, 79962, 79963, 79964, 80126, 80127, 80128, 80139, 80141, 80150, 80152, 80304, 80312